Monte Carlo study of freezing of polydisperse hard spheres

Peter G. Bolhuis
FOM Institute for Atomic and Molecular Physics, Kruislaan 407, 1098 SJ Amsterdam, The Netherlands

David A. Kofke
Department of Chemical Engineering, State University of New York at Buffalo, Buffalo, New York 14260-4200
(Received 28 February 1996)

We have established the solid-fluid coexistence region for a system of polydisperse hard spheres with near Gaussian diameter distributions, as a function of polydispersity. Our approach employs Monte Carlo simulation in the isobaric semigrand ensemble with a Gaussian activity distribution. Gibbs-Duhem integration is used to trace the coexistence pressure as a function of the variance of the imposed activity distribution. Significantly, we observe a ''terminal'' polydispersity above which there can be no fluid-solid coexistence. The terminus arises quite naturally as the Gibbs-Duhem integration path leads the pressure to infinity. This pressure divergence is an artifact of the method used to evaluate the freezing transition, because the sphere diameters vanish in this limit. A simple rescaling of the pressure with the average diameter brings the terminal pressure to a finite value. Nevertheless, the existence of this terminus only at infinite pressure precludes the construction of a continuous path from the solid to the fluid. At the terminus the polydispersity is 5.7% for the solid and 11.8% for the fluid while the volume fractions are 0.588 and 0.547 for the solid and fluid, respectively. Substantial fractionation observed at high values of the polydispersity ($>5\%$) implies that the ''constrained eutectic'' assumption made in previous theoretical studies is not generally valid. Our results for the terminal polydispersity are consistent with experiments performed on polydisperse colloidal suspensions. [S1063-651X(96)05007-6]

PACS number(s): 82.20.Wt, 64.60.Cn, 82.70.Dd

I. INTRODUCTION

Systems interacting via purely repulsive hard potentials are of interest because their properties have a trivial dependence on temperature, they are theoretically tractable, and they capture the qualitative effects of intermolecular repulsion on material properties. These models are particularly good at characterizing the structural features of condensed phases [1]. While they are incapable of exhibiting vapor-liquid transitions, properly formulated models have been shown to exhibit a rich array of order-disorder transitions, including freezing [2,3], polymorphism (in hard-sphere mixtures) [4–6], and liquid crystalline phases [7–9] (seen, for example, in hard spherocylinders).

The hard-sphere model gives a very good description of colloidal dispersions that consist of noncharged spherical particles interacting via a steep steric repulsion [10]. In particular, such colloidal systems, if sufficiently monodisperse in size, are known to crystallize at densities very close to that predicted by a hard-sphere model [11]. However, colloidal particles frequently exhibit considerable size polydispersity, depending on the way they are synthesized. This polydispersity will affect the thermodynamic properties, including the location and existence of any phase transitions.

The influence of polydispersity on the solid-fluid transition in colloidal suspensions was first examined by Dickinson and Parker [12–14]. Their system consisted of particles interacting via a screened Coulombic repulsion with a van der Waals attractive term. They showed via molecular simulation that the osmotic pressure of this system varies significantly with size polydispersity. They estimated the solid-fluid coexistence properties as a function of the polydispersity, but without attempting any sort of rigorous free energy calculations or considering the possibility of size fractionation (i.e., they assumed that the particle diameter distributions in the coexisting solid and fluid phases are identical). They found that the fluid-solid coexistence region narrows as the polydispersity increases, and they surmised that the transition disappears entirely at sufficiently high polydispersity. This value of the polydispersity has been called by Dickinson and Parker the ''critical polydispersity''; this choice is unfortunate as the phenomenon does not likely represent a continuous transition because the solid and fluid phases have different symmetries. To avoid any confusion with critical points as they are customarily understood, we will instead refer to this polydispersity as the ''terminal polydispersity.''

The terminal polydispersity has come to be the subject of considerable interest. For a triangular size distribution, Dickinson and Parker extrapolated the change in volume upon melting to zero, and estimated the terminal polydispersity at 11% (we define the polydispersity as the standard deviation of the particle size distribution, divided by the mean). Later, Pusey [15] proposed a simple criterion for the terminal polydispersity based on an analogy of the Lindemann melting criterion; he also obtained a value of about 11%. Pusey [11] performed experiments in which he observed that dispersions with a polydispersity of 7.5% would (partly) freeze, while those with a polydispersity of 12% did not.

Several authors applied density functional theory (DFT) to obtain the phase diagram of polydisperse hard spheres [16,17]. These theories are significantly more sophisticated than those employed in prior studies, and they give more attention to free energy criteria in calculating the coexistence

curves. They nevertheless do not represent a completely rigorous treatment, as they too do not consider the effect of fractionation on the coexistence properties. McRae and Haymet [17] refer to this approximation as a ''constrained eutectic.'' The constrained eutectic is certainly valid at small polydispersity, but it likely breaks down as the distribution of diameters becomes wide. The DFT studies predict the terminal polydispersity at about 5–6%.

The purpose of the present work is to determine rigorously the phase diagram of polydisperse hard spheres by molecular simulation, establish the terminal polydispersity, and test the validity of the constrained eutectic assumption made explicit in Ref. [17]. To do this properly we must simulate a system having a truly continuous distribution of particle sizes, rather than a many-component but nevertheless discrete distribution. Such a simulation can be realized in the so-called semigrand ensemble, which has the added advantage that it is well suited for calculation of multicomponent phase equilibria. The semigrand ensemble is explained in Sec. II. Section III describes how the recently developed Gibbs-Duhem integration method [18] can be applied to efficiently obtain the phase diagram of polydisperse hard spheres by integration along the coexistence line. To start the integration one needs the slope of the coexistence line in the monodisperse limit; the means by which this is obtained is described in Sec. IV. In Sec. V, it is shown how scaling properties of the system can be applied to greatly improve the accuracy of the simulations. The simulation results are discussed in Sec. VI. The existence of a terminal polydispersity raises questions of continuity of the fluid and solid states; we show in Sec. VII how this issue may be resolved. Concluding remarks are presented in Sec. VIII.

II. SEMIGRAND ENSEMBLE

The most straightforward approximation to a continuous mixture is based in the canonical ensemble and thus takes a finite sample from a distribution of diameters $p(\sigma)$. However, this approach is sensitive to finite size effects and, moreover, it is not practical when phase equilibria are considered as it is difficult to ensure chemical potential equilibration of each component. A better choice is a grand canonical simulation in which particles of different species are inserted and removed according to the configurational energy and the *imposed* chemical potential of that component. In this way a truly continuous distribution can be realized and phase equilibrium can be more easily treated. However, at the high densities of the liquid-solid equilibrium the insertion probability in both phases is too low to obtain reasonable statistics; further, the need to maintain the crystal structure in the solid makes insertions especially problematic.

The semigrand ensemble provides an alternative representation that combines the best features of the canonical and grand canonical ensembles for the study of continuous mixtures [19,21]. A simulation in this ensemble has the total number of particles fixed, but the species identity of each particle is allowed to change, giving rise to a truly continuous distribution. Although the chemical potentials are imposed in a way similar to the grand-canonical ensemble, insertion of particles is avoided, so the method is suitable for high densities and crystalline phases.

We consider a system of N hard spheres with diameters σ distributed according to $p(\sigma)$. The isobaric semigrand canonical free energy Y is defined by a Legendre transform of the Gibbs free energy G. In the polydisperse limit,

$$Y=G-N\int p(\sigma)[\mu(\sigma)-\mu(\sigma_0)]d\sigma=N\mu(\sigma_0) \quad (1)$$

or, in differential form,

$$d(\beta Y)=Hd\beta+\beta VdP-N\int p(\sigma)\beta\delta[\mu(\sigma)-\mu(\sigma_0)]d\sigma + \beta\mu(\sigma_0)dN. \quad (2)$$

Here, $\mu(\sigma)$ is the chemical potential as a function of σ, σ_0 is the diameter of an arbitrarily chosen reference component, and δ represents a functional differential. Also, H is the enthalpy, $\beta=1/k_BT$ is the reciprocal temperature, P is the pressure, and V the volume of the system. The semigrand canonical potential Y is a function of the independent variables T, V, and N and it is a functional of the chemical potential difference function $\mu(\sigma)-\mu(\sigma_0)$. In a simulation these independent variables must be fixed while the thermodynamic conjugates $U,P,\mu(\sigma_0)$ and $p(\sigma)$ are allowed to fluctuate. This implies that the composition $p(\sigma)$ can be known only after the simulation has been performed. Because the total number of particles is fixed the chemical potential of the reference $\mu(\sigma_0)$ still has to be computed. Once it is determined, the entire chemical potential distribution is known. The method is therefore well suited for phase equilibria in continuous mixtures: for a given temperature and distribution in chemical potential differences one needs to match only the values of the pressure and the reference chemical potential in both phases. This is far simpler than matching the entire distribution $\mu(\sigma)$ in the canonical way.

We are interested in determining the influence of polydispersity on the hard sphere fluid-solid transition. Although the composition distribution and hence the polydispersity cannot be imposed directly, it can be expected that its form will be much like that of the imposed activity-ratio distribution $e^{\beta[\mu(\sigma)-\mu(\sigma_0)]}$ [21]. Therefore we choose the following quadratic form for the chemical potential difference function

$$\beta[\mu(\sigma)-\mu(\sigma_0)]=-(\sigma-\sigma_0)^2/2\nu, \quad (3)$$

which gives rise to a Gaussian activity distribution that peaks at $\sigma=\sigma_0$, with width ν. In the limit $\nu\to 0$, the pure monodisperse σ_0 phase is recovered. For small ν the mixture is ideal and the composition will be Gaussian with the peak near σ_0. The choice of Eq. (3) converts Y from a functional of $\mu(\sigma)-\mu(\sigma_0)$ to a function of σ_0 and ν. The fundamental thermodynamic equation now reads

$$d(\beta Y)=Hd\beta+\beta VdP+\beta\mu(\sigma_0)dN-(Nm_1/\nu)d\sigma_0 - (Nm_2/2\nu^2)d\nu, \quad (4)$$

where m_1 and m_2 are the first and second moments of the composition about σ_0. The nth such moment is defined as

$$m_n=\int d\sigma(\sigma-\sigma_0)^n p(\sigma). \quad (5)$$

In a semigrand Monte Carlo simulation, particles sample diameters in addition to the usual sampling of positions within the simulation box. Diameters are sampled by selecting a particle at random, changing its diameter by a small amount, and accepting with probability in accord with the Metropolis algorithm. Details may be found in [20].

III. GIBBS-DUHEM INTEGRATION

Evaluation of the hard-sphere fluid-solid coexistence line as a function of polydispersity can be done by application of the Gibbs-Duhem integration method recently developed by one of the authors [18]. In this method two phases are simulated simultaneously at the same state conditions. The technique allows a series of simulations to trace a line of coexistence in the plane of two state variables; for the purpose of describing the method let us say that these variables are the temperature and pressure, respectively. Chemical potential equality between the phases is ensured by starting the process with two known equilibrium phases, and subsequently applying thermodynamic integration to select the appropriate pressure while the temperature is varied from one simulation to the next in the series. The integration path may be derived from the Gibbs-Duhem equation

$$d(\beta\mu) = h\,d\beta + \beta v\,dP, \tag{6}$$

where $h = H/N$ and $v = V/N$ are the molar enthalpy and volume, respectively. For two coexisting phases to remain in equilibrium when the temperature is changed, the pressure must vary in a way that maintains chemical potential equality between them. The required change can be derived from Eq. (6)

$$\left(\frac{dP}{d\beta}\right) = -\frac{\Delta h}{\beta \Delta v}, \tag{7}$$

where Δ indicates a difference between the two phases. Equation (7) is known as the Clapeyron equation. It is a simple first-order differential equation which can be integrated using a predictor-corrector scheme. The ''initial condition'' is a known point at the coexistence line in the (T,P) plane. By simulating the two coexisting phases simultaneously at the equilibrium pressure and evaluating the right-hand side of Eq. (7), one can predict the pressure at another temperature not far away. Simulation at this P and T yields new values of Δh and Δv, which can be used to correct the predicted pressure while the simulation continues to proceed. The process is then repeated to get the next (T,P) coexistence state point. Details of the method may be found elsewhere [18,22]. In the case of polydisperse hard spheres we do not need the temperature as an independent variable, but instead we need a measure for the polydispersity. An obvious choice is ν, as it occurs in the fundamental Eq. (4). The Gibbs-Duhem equation for polydisperse mixtures can be derived by combining $Y = \mu(\sigma_0)N$ with Eq. (2)

$$d[\beta\mu(\sigma_0)] = h\,d\beta + \beta v\,dP - \int p(\sigma)\beta\delta[\mu(\sigma) - \mu(\sigma_0)]\,d\sigma. \tag{8}$$

Using the same procedure as for the derivation of Eq. (4) we obtain

$$d[\beta\mu(\sigma_0)] = h\,d\beta + \beta v\,dP - (m_1/\nu)\,d\sigma_0 - (m_2/2\nu^2)\,d\nu. \tag{9}$$

To ensure phase equilibrium, $\beta\mu(\sigma_0)$ and the chemical potential difference function given in Eq. (3) must be the same in the two phases. The latter requirement is fulfilled simply by using the same ν (and σ_0) in both phases. The first requirement results in a Clapeyron type of equation which can be derived from Eq. (9) by equating the right-hand side for both phases and applying $d\sigma_0 = 0$ and $d\beta = 0$.

$$\left(\frac{dP}{d\nu}\right) = \frac{\Delta m_2}{2\nu^2 \beta \Delta v}. \tag{10}$$

We can integrate in the (P,ν) plane by measuring the second moment of the composition distribution m_2 and the molar volume v in both phases and applying the predictor-corrector scheme described above.

IV. THE INITIAL SLOPE

The starting point we use for the Gibbs-Duhem integration is the well known freezing point of monodisperse hard spheres [2,3]. However, the initial slope at $\nu = 0$ given by Eq. (10) is not known here. Moreover, it cannot be calculated directly in a simulation because both m_2 and ν are equal to zero in the monodisperse limit, although the ratio m_2/ν is expected to be finite.

The second moment m_2 can be calculated if the composition $p(\sigma)$ is known. The composition in turn is related to the chemical potential by

$$\beta\mu(\sigma) = \mu^0 + \ln p(\sigma) + \beta\mu_r(\sigma), \tag{11}$$

where μ^0 is a collection of terms taken as independent of σ, and $\beta\mu_r(\sigma)$ is the residual chemical potential. With Eq. (3), the chemical potential difference function can now be written as

$$\beta\Delta\mu(\sigma) = \ln\frac{p(\sigma)}{p(\sigma_0)} + \beta\Delta\mu_r(\sigma) = -\frac{(\sigma-\sigma_0)^2}{2\nu}, \tag{12}$$

or

$$p(\sigma) \sim \exp[-(\sigma-\sigma_0)^2/(2\nu) - \beta\Delta\mu_r(\sigma)]. \tag{13}$$

Here, $\Delta\mu_r(\sigma) = \mu_r(\sigma) - \mu_r(\sigma_0)$ is the difference in residual chemical potential between a particle with diameter σ and a particle of the reference component. This difference can be measured in a simulation of a pure σ_0 substance by performing ''test enlargements,'' in which a randomly chosen particle is enlarged from diameter σ_0 to a random diameter σ. One tabulates the frequency with which such moves result in

no overlap, although the moves themselves are never accepted. This overlap probability yields the residual chemical potential according to

$$\beta\Delta\mu_r(\sigma) = -\ln\langle\exp[-\beta\Delta U(\sigma_0\rightarrow\sigma)]\rangle, \tag{14}$$

where the brackets indicate the ensemble average; $\exp(-\beta\Delta U)$ is zero or unity, respectively, corresponding to the absence or presence of overlap. This ''ghost-growing'' procedure is very similar to the Widom ''ghost'' particle insertion technique [23]. In practice we tabulate the distance from a randomly selected particle to its nearest neighbor; this histogram of nearest distances is then easily converted into the overlap histogram just described.

For small values of $\sigma-\sigma_0$ the measured residual chemical potential might be approximated by a quadratic function

$$-\beta\Delta\mu_r(\sigma) = a_1(\sigma-\sigma_0)+a_2(\sigma-\sigma_0)^2. \tag{15}$$

Substituting this in Eq. (13) results in the composition

$$p(\sigma) = C\exp\left[a_1(\sigma-\sigma_0)+\left(a_2-\frac{1}{2\nu}\right)(\sigma-\sigma_0)^2\right], \tag{16}$$

where C is independent of $\sigma-\sigma_0$. Because $p(\sigma)$ is a Gaussian function, the desired second moment of the composition m_2 can be analytically obtained

$$m_2 = \frac{1+a_2/(1/\nu-2a_2)}{(1/\nu-2a_2)} \approx \nu+(a_1^2+2a_2)\nu^2. \tag{17}$$

The latter approximation is correct to the second order in ν. The initial slope can now be written as

$$\left(\frac{dP}{d\nu}\right)_{\nu=0} = \frac{\Delta m_2}{2\nu^2\beta\Delta v} = \frac{\Delta\left(\frac{1}{2}a_1^2+a_2\right)}{\beta\Delta v}, \tag{18}$$

where $\Delta[(\frac{1}{2}a_1^2+a_2)]$ is the difference between the coefficient expressions evaluated in both phases. In sum, we measure the residual chemical potential in a simulation of a pure hard-sphere system using Eq. (14), we fit it to a quadratic function for small $\sigma-\sigma_0$ and use the coefficients in Eq. (18) to obtain the initial slope for the Gibbs-Duhem integration.

V. SCALING

Application of a standard Monte Carlo algorithm yielded very poor statistics. This outcome is probably caused by the inability of the volume to adjust quickly to particle diameter changes, and vice versa. A remedy might be to introduce a combined volume and diameter-change Monte Carlo step: while reducing the volume by a factor α, we reduce all diameters by a factor $\alpha^{1/3}$. In addition to more directly coupling the diameter and volume changes, this move is appealing because it requires no overlap test. The acceptance probability for this combined move is

$$P_{L\rightarrow L'} = \exp\Bigg[\beta P(L'^3-L^3)-3N\ln(L'/L) + \frac{1}{2\nu}\sum_i(\tilde{\sigma}_iL'-\sigma_0)^2-\frac{1}{2\nu}\sum_i(\tilde{\sigma}_iL-\sigma_0)^2\Bigg], \tag{19}$$

where L is the length of the cubic box with volume $V=L^3$ and $\tilde{\sigma}_i=\sigma_i/L$ are the scaled diameters. Although this method will produce better results, we can improve the scheme even more by scaling both the diameters and the coordinates, thereby permitting (near-) analytic evaluation of the volume integral. Consider the configurational part of the isobaric semigrand partition function

$$\Upsilon = \frac{1}{N!}\int dr^N\int d\sigma^N\int dV\exp\Bigg[-\beta PV+\frac{1}{2\nu}\sum_i(\sigma_i-\sigma_0)^2 - \beta U(r^N,\sigma^N)\Bigg]. \tag{20}$$

If we now introduce scaled coordinates and diameters $s_i=r_i/L$ and $\tilde{\sigma}_i$ as above the partition function can be written as

$$\begin{aligned}\Upsilon &= \int ds^N\int d\tilde{\sigma}^N e^{-\beta U(s^N,\tilde{\sigma}^N)}\int dL^3L^{4N}\exp\Bigg[-\beta PL^3 + \frac{1}{2\nu}\sum_i(\tilde{\sigma}_iL-\sigma_0)^2\Bigg]\\ &= \int ds^N\int d\tilde{\sigma}^N e^{-\beta U(s^N,\tilde{\sigma}^N)}W(\tilde{\sigma}^N).\end{aligned} \tag{21}$$

The outermost two integrals do not contain any volume dependence. Moreover, the ''weighting function'' $W(\tilde{\sigma}^N)$ defined here can be evaluated entirely at every Monte Carlo move. In this way, there is no need for volume sampling at all. Instead, at every move we obtain the average volume by evaluating

$$\frac{\int dLL^{4N+5}\exp\left[-\beta PL^3+\frac{1}{2\nu}\Sigma_i(\tilde{\sigma}_iL-\sigma_0)^2\right]}{\int dLL^{4N+2}\exp\left[-\beta PL^3+\frac{1}{2\nu}\Sigma_i(\tilde{\sigma}_iL-\sigma_0)^2\right]}. \tag{22}$$

In this scaling method there are only two kinds of Monte Carlo moves: the regular particle displacements and the diameter changes. Both changes are made in the scaled variables. The acceptance probabilities are

$$P_{s_i\rightarrow s_i'} = e^{-\beta\Delta U(s^N,\tilde{\sigma}^N)}, \quad P_{\tilde{\sigma}_i\rightarrow\tilde{\sigma}_i'} = e^{-\beta\Delta U(s^N,\tilde{\sigma}^N)}\frac{W(\tilde{\sigma}_i')}{W(\tilde{\sigma}_i)}, \tag{23}$$

where $\Delta U(s^N,\tilde{\sigma}^N)$ is the change in potential energy associated with the move. If a particle's diameter is changed the integral $W(\tilde{\sigma}^N)$ must be reevaluated. Because the exponential in the integral is a cubic polynomial this cannot be done analytically. However, if we write the integral as

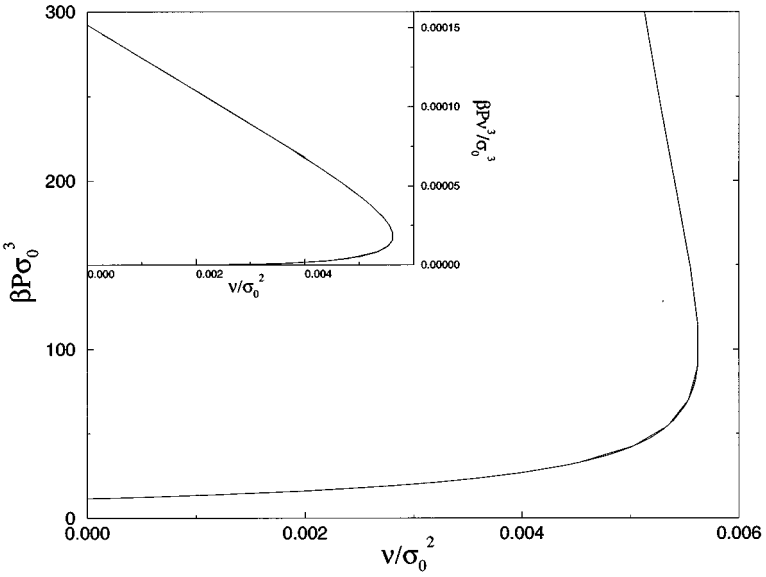

FIG. 1. Solid-fluid coexistence pressure as a function of variance of the imposed activity distribution. In the inset the pressure is reduced to $P\nu^3/\sigma_0^3$ to show the limiting behavior.

$$W(\tilde{\sigma}^N) = c\int dx e^{f(x)} \tag{24}$$

we can approximate it accurately by applying the method of steepest descent. Replacing the function $f(x)$ by a second-order Taylor expansion around the maximum of $f(x)$ yields

$$W(\tilde{\sigma}^N) = c\int dx \exp\left[f(x_{max}) + \frac{1}{2}\left(\frac{\partial^2 f}{\partial x^2}\right)_{x_{max}} (x-x_{max})^2 \right]$$

$$= c e^{f(x_{max})}\left[-2\pi\left(\frac{\partial^2 f}{\partial x^2}\right)^{-1}_{x_{max}} \right]^{1/2}. \tag{25}$$

This approximation is possible because the function $f(x)$ (being proportional to N) is sharply peaked about its maximum.

VI. RESULTS

We performed a Gibbs-Duhem integration in the (P,ν) plane starting with an fcc solid and a fluid at the monodisperse hard-sphere freezing point. Both systems consisted of 256 particles and were well equilibrated. Using the ghost-growing method of Sec. IV in combination with Eq. (18) we found an initial slope of $dP/d\nu = 1400(\pm 50)$ (in units such that β and σ_0 are unity). This value was used in the first predictor step to go from $\nu = 0$ to finite ν, where the slope could be directly measured. We evaluated the coexistence line by gradually increasing ν from one simulation to the next while integrating Eq. (10) to determine the pressure. In Fig. 1 the equilibrium pressure is shown as a function of the polydispersity parameter ν. The slope starts off at a value of $dP/d\nu = 1400$ as we obtained from Eq. (18) and increases when ν is increased. At a value of $\nu/\sigma_0^2 = 0.0056$ the slope becomes infinite, so we had to invert the integration, taking P as the independent variable. In this case, we can calculate $\nu(P)$ for increasing values of P by applying the same integration scheme to the reciprocal of Eq. (10). Surprisingly, the equilibrium curve continues to bend back, approaching $\nu/\sigma_0^2 = 0$ at infinite pressure. In the inset of Fig. 1 we rescale the pressure to $\tilde{P} = \beta P \nu^3/\sigma_0^3$, which remains finite and follows a straight line as $P \to \infty, \nu/\sigma_0^2 \to 0$. The fact that $\tilde{P}$ is finite in this limit actually allows us to perform simulations at infinite pressure as will be discussed in the next section.

The divergence of the pressure is somewhat misleading. The pressure indeed goes to infinity on a scale characterized by σ_0, but when reduced instead by the volume or an average diameter it remains bounded. In fact, in this limit σ_0 loses its relevance as a length scale because all particle diameters are going to values much smaller than σ_0. Scaling by an average diameter (or the volume) makes the interpretation of the results more intuitive because in experiments the important microscopic length scale is the characteristic particle diameter. Consequently, in most of what follows we present our results in terms of $\langle\sigma\rangle$ (where the angle brackets indicate an isobaric semigrand ensemble average). We choose arbitrarily to use $\langle\sigma\rangle$ of the solid to perform the reduction; we could just as well have used the fluid value. We will continue to refer to the limit of infinite pressure because this represents a limiting behavior of our isobaric semigrand system. It should be understood that in this case the pressure is infinite on the σ_0 scale but not on, say, the $\langle\sigma\rangle$ scale.

Although the parameter ν shows a maximum as a function of P, the real polydispersity—given in terms of the width of the composition distribution $p(\sigma)$—does not. This polydispersity s is defined as

$$s = \frac{\langle\sigma^2\rangle}{\langle\sigma\rangle^2} - 1. \tag{26}$$

In Fig. 2 the reduced pressure $\beta P\langle\sigma\rangle^3_{\text{solid}}$ is plotted against the polydispersity s in both the fluid and the solid. The equilibrium pressure increases monotonically until at infinite pressure a limiting value of s and $\beta P\langle\sigma\rangle^3$ is reached. From this plot it becomes immediately clear that the polydispersity of the fluid and the solid at equilibrium can be very different. As reviewed in the Introduction, this fact, although anticipated, was discounted in previous studies.

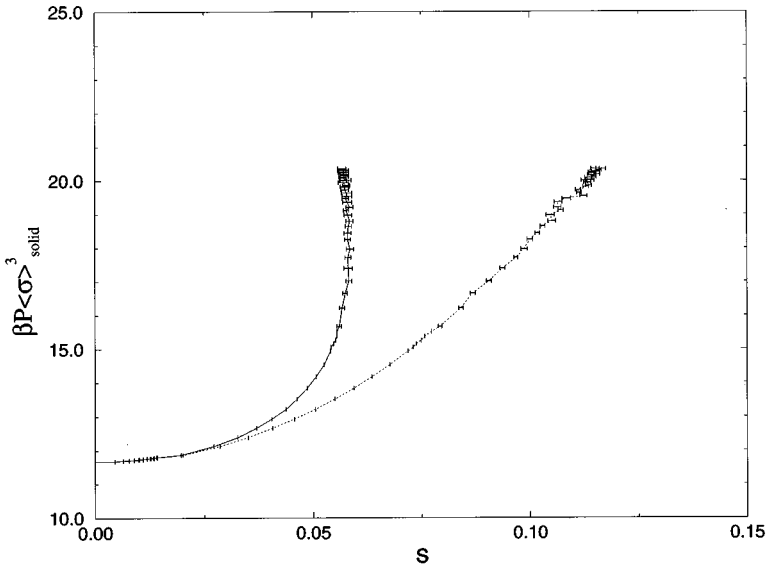

FIG. 2. Coexistence pressure of the solid (left curve) and the fluid (right curve) as a function of the width of the composition distribution, the polydispersity s.

It is convenient to choose a density variable η given in terms of the real volume fraction, because this is the quantity one measures in experiments. We define $\eta = N\pi\langle\sigma^3\rangle/(6V)$; note that $\eta = 0.7405$ for monodisperse close packed spheres. The phase diagram in the (η, s) plane is shown in Fig. 3. Because the polydispersity variable is not linearly additive, the tie lines are curved. Coexisting fluid and solid hard spheres will mix to density-polydispersity values given by the lines (the converse is not necessarily true, as there are many compositions possible for a particular s, and an arbitrary one may not split exactly to the coexisting phases computed for the diagram). The most remarkable feature of the diagram is the fact that the fluid-solid equilibrium suddenly ends. This is generally consistent with the prediction and observation of a terminal polydispersity reported in studies on crystallization of polydisperse hard spheres [11,17,16] and reviewed in the Introduction. In particular, the consensus of a terminal polydispersity in the range of 5%–12% is explained by our results. According to our phase diagram, the fcc solid phase is thermodynamically stable for polydispersities no more than 5.7%, yet crystallization is possible in fluids of polydispersity up to 12% provided one allows for fractionation in the phase separation process. This is consistent with Pusey's experiments [11] in which he observed that dispersions with a polydispersity of 7.5% would freeze, while those with a polydispersity of 12% did not. The DFT studies which reported a terminal polydispersity of 5–7% are also consistent with our results given their use of the constrained eutectic, which precludes fractionation.

In Fig. 4, we plot the number density (in units of the average diameter) as a function of s. This plot illustrates the counterintuitive result that the fluid density may adopt values greater than that in the solid phase. At the point where both densities are equal the Δv term in Eq. (10) switches signs and becomes negative, which gives rise to the maximum of $\nu(P)$ seen in Fig. 1. Of course, the fluid is able to take on larger densities than the solid only because it is composed of particles of smaller diameter.

The composition distributions of the fluid and the solid phases are displayed in Fig. 5 for four values of the coexist-

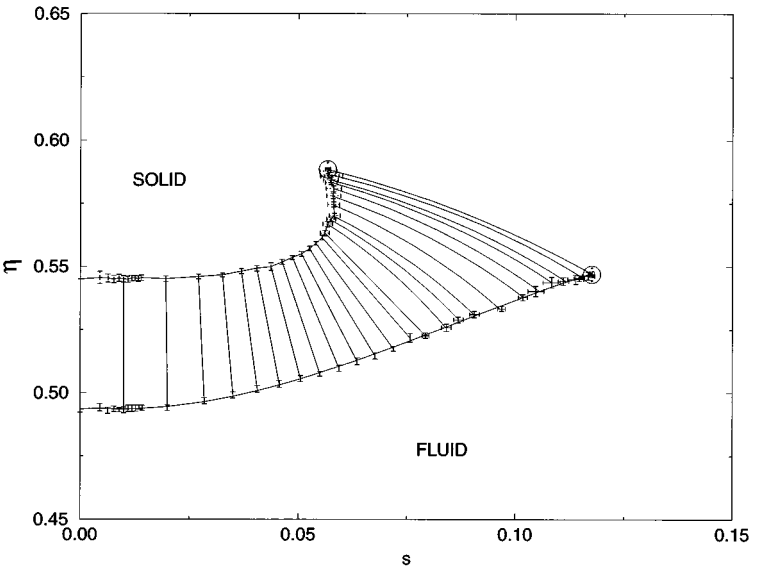

FIG. 3. Phase diagram in the plane of volume fraction and polydispersity. Coexisting phases are joined by tie lines, which are not straight because the polydispersity is not an additive variable. The circles represent the end points of the coexistence region at $\beta P\sigma_0^3 \to \infty$, i.e., the terminal polydispersity.

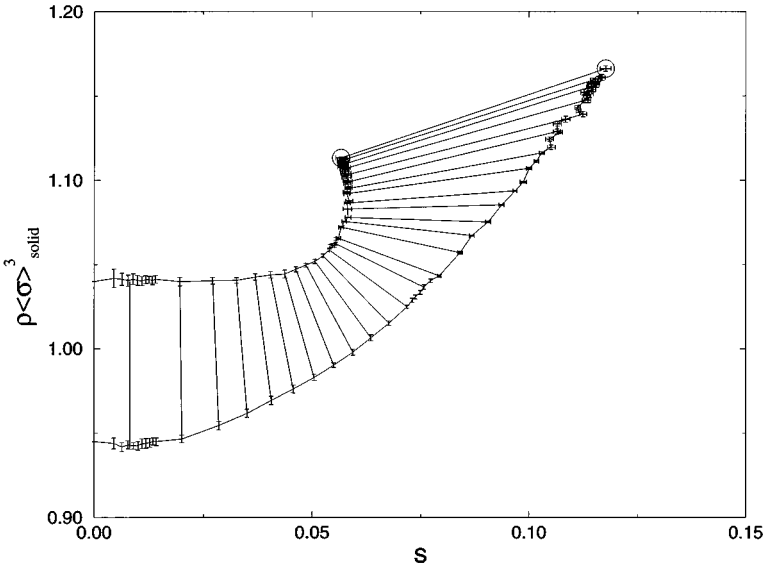

FIG. 4. Phase diagram in the plane of reduced number density and polydispersity. Coexisting phases are joined by tie lines, which although curved in reality are rendered straight in this figure.

ence pressure. For a monodisperse equilibrium (not shown in the figures) the distributions in both phases would be equal to the imposed activity, which is a δ function at σ_0. As the equilibrium pressure (or equivalently the value of ν) is increased, the composition distributions depart from the ideal activity. Although still almost Gaussian, they are shifted considerably to lower values of σ. The average diameter is smaller in the fluid, whereas the solid composition is located at larger diameters and is more narrowly distributed. The difference between the phases becomes more pronounced at higher pressures. At infinite pressure, all diameters go to zero on the scale of σ_0. Interesting distributions can be recovered by proper scaling of the diameters by their average, as presented in Fig. 5(d). The fluid distribution is much broader than the solid one, in accord with the larger polydispersity s we encountered above. Although the value ν/σ_0^2 has decreased to zero in this limit (and of course has the same value in the two phases), the (rescaled) composition distributions are still near-Gaussian with a finite width (on a scale of $\langle\sigma\rangle$). This curious outcome is a result of the limiting process in which $\beta P\sigma_0^3\to\infty$ while $\nu/\sigma_0^2\to 0$.

As the distributions are shifted to a lower diameter at a high pressure, the precise shape of the imposed activity distribution becomes less important and σ_0, as discussed above, becomes irrelevant. In Fig. 5(c) the chemical potential difference function, the logarithm of the activity, is nearly a straight line; it becomes exactly a straight line in the infinite pressure limit. This property enables us to perform simulations in the limit of $\beta P\sigma_0^3\to\infty$.

VII. THE INFINITE PRESSURE LIMIT

The existence of the terminal polydispersity suggests the possibility of constructing a continuous path from the solid

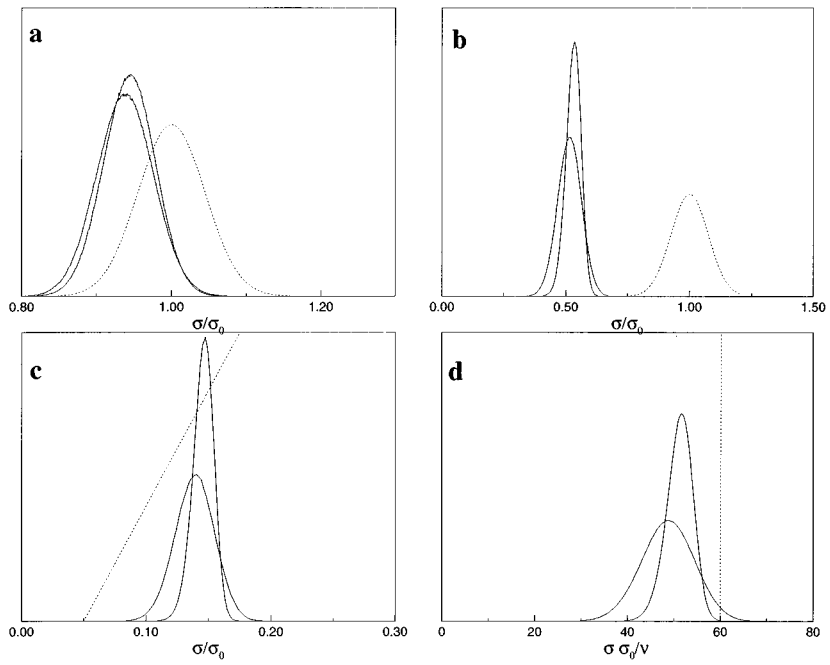

FIG. 5. Composition distributions $p(\sigma)$ for fluid-solid equilibrium at different pressures. In the figures, the leftmost solid curve represents the fluid composition, the rightmost one the solid phase composition. (a) $p(\sigma)$ for $\beta P\sigma_0^3=15$. The dotted curve is the imposed (Gaussian) activity distribution. (b) $p(\sigma)$ for $\beta P\sigma_0^3=100$. The dotted curve is the imposed (Gaussian) activity distribution. (c) $p(\sigma)$ for $\beta P\sigma_0^3=6400$. The dotted line denotes the imposed chemical potential difference function, which is becoming straight at high βP. (d) $p(\sigma\sigma_0/\nu)$ for $\beta P\sigma_0^3\to\infty$. In this limit the diameter are pushed to zero. By dividing them by ν/σ_0 they remain finite. The dotted line denotes the imposed chemical potential difference function.

TABLE I. Polydispersities, densities, and volume fractions of the solid fluid equilibrium at $\beta P\sigma_0^3\to\infty$. The subscript numbers indicate the error in the last digit(s).

	Solid	Fluid
s	0.0567_{12}	0.1176_{12}
$\rho\langle\sigma\rangle^3_{\text{solid}}$	1.1131_{7}	1.1662_{16}
η	0.5884_{7}	0.5468_{13}

to fluid without going through a first-order phase transition. We do not expect such a process to be realizable in general, and in this section we show that it is indeed not possible in the context of our system. The explanation lies in the infinite pressure limiting behavior of the model in the isobaric semigrand ensemble.

Consider the partition function of Eq. (21)

$$\Upsilon=\int ds^N\int d\tilde{\sigma}^N e^{-\beta U(s^N,\tilde{\sigma}^N)}\int dL^3L^{4N}\exp\Bigg[-\beta PL^3+\frac{1}{2\nu}\sum_i(\tilde{\sigma}_iL-\sigma_0)^2\Bigg]. \tag{27}$$

In the limit of $\beta P\sigma_0^3\to\infty$ the volume and hence the length L will go to zero. The quadratic term in L in the exponent vanishes in this limit, whereas the βPL^3 and the $L\sigma_0/\nu$ terms remain finite. This is equivalent to the observation that the chemical potential difference function is becoming a straight line. If we define a new, always finite, parameter $x=L\sigma_0/\nu$ and introduce $\tilde{P}$ defined above, the limiting partition function can be written as

$$\Upsilon=C\int ds^N\int d\tilde{\sigma}^N e^{-\beta U(s^N,\tilde{\sigma}^N)}\int dx x^{4N}\exp\Bigg[-\tilde{P}x^3+\Bigg(\sum_i\tilde{\sigma}_i\Bigg)x\Bigg]. \tag{28}$$

We can conduct simulations in the infinite pressure limit by using the integral over x as the ''weighting function'' $W(\tilde{\sigma}^N)$ and imposing the reduced pressure $\tilde{P}$. This limiting state is governed by two length scales, namely $(\beta P)^{-1/3}$ and ν/σ_0. The pressure βP drives the diameters to smaller values whereas ν/σ_0 drives them to large ones [σ_0/ν is equal to the now-constant slope of $\Delta\mu(\sigma)$ as is shown in Fig. 5(d)]. The ratio of these two lengths, as expressed via $\tilde{P}$, represents the balance between the two forces.

The reduced coexistence pressure can be obtained from extrapolation of $\tilde{P}$ to $\nu/\sigma_0^2=0$ as suggested by Fig. 1. The equilibrium densities and volume fractions of the solid-fluid coexistence in the limit $\beta P\sigma_0^3\to\infty$ are displayed as open circles in Figs. 4 and 3, respectively and are given in Table I. Because these equilibrium points are at infinite pressure, these are really the end points of the phase coexistence. For the choice of the chemical potential distribution given by Eq. (3), there is no fluid-solid phase transition at higher polydispersities, volume fractions or densities.

This method makes it possible to address the question of solid-fluid phase continuity posed above: given that the coexistence region terminates abruptly, why is it not possible to go from the solid to the fluid via a continuous path in the (η,s) plane, that is, without encountering a first-order phase transition? The answer is made clear by simulations at other, off-coexistence values of the reduced pressure $\tilde{P}$. The results are included in Fig. 6. The curve bounding the solid region from monodisperse close packing $(s=0,\eta=1)$ to the solid-fluid coexistence represents the infinite pressure line; a similar curve is shown for the fluid phase (let us call these curves the ''$\tilde{P}$ lines''). The $\tilde{P}$ lines provide an upper limit, above which the system cannot be compressed. This upper bound implies that it is not possible to go from the solid to the fluid avoiding a first-order transition.

Although all semigrand $\tilde{P}$ states are of infinite pressure, the $\tilde{P}$ line does not correspond to close-packed states one would achieve in a canonical ensemble. The linear chemical potential that arises in the infinite pressure limit is incapable of producing the tight packing one normally associates with infinite pressure (i.e., in a fixed-composition ensemble). In order to determine the maximum volume fraction η_M of the solid phase as a function of polydispersity, we performed

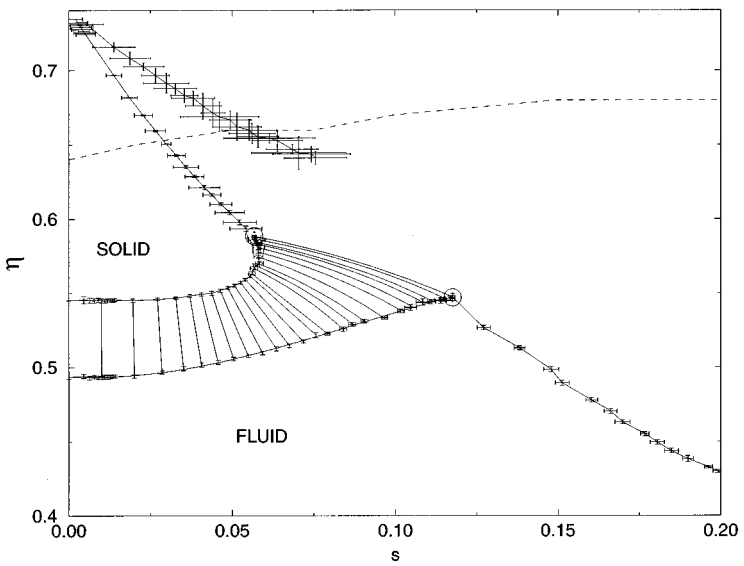

FIG. 6. Phase diagram of polydisperse hard spheres in the η-s plane. The coexistence region is as in Fig. 3. The curve joining the terminal solid-phase coexistence point to the $s=0$ closed-packed limit is the solid-phase $\tilde{P}$ line (see text), while that emanating from the liquid-phase terminus is the liquid-phase $\tilde{P}$ line. The solid line above the solid-phase $\tilde{P}$ line describes the packing fractions obtained from the fixed-composition compressions described in the text. Fluid-phase random close packing obtain by Schaertl and Sillescu [25] is described by the dashed curve.

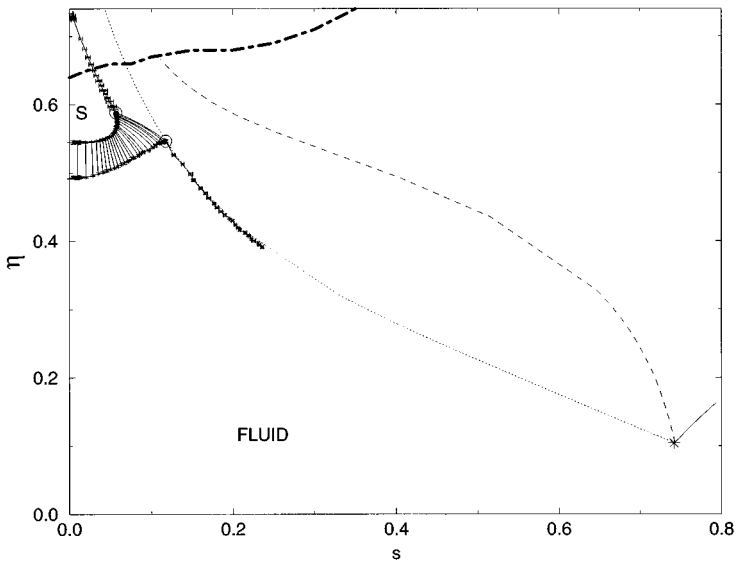

FIG. 7. Behavior of polydisperse hard spheres in the η-s plane. Phase diagram, $\tilde{P}$ lines, and random-close packing curves from Fig. 6 are included. Fluid-phase curves according to the Mansoori *et al.* [24] equation of state are presented for chemical potential distributions linear (dotted curve), quadratic (dashed curve), and cubic (solid curve) in the sphere diameter. The three lines converge at the infinitely polydisperse limit, for which a Monte Carlo datum [26] is indicated.

simulations starting with a configuration obtained by semigrand simulation at the $\tilde{P}$ line and compressing at fixed composition until every particle was constrained by its neighbors. The maximum volume fraction η_M so obtained was averaged over ten different starting configurations with a different diameter distribution snapshot. These averaged η_M as a function of polydispersity are included in Fig. 6. It is immediately clear that there is a large difference between the semigrand $\tilde{P}$ curve and the canonical results for η_M. Simulations of larger systems indicate that this is not a finite-size effect. The explanation is that the imposed linear chemical potential difference function in the semigrand simulations is simply not the one that produces the maximum volume fraction η_M. To remove the difference between the canonical and semigrand picture one could study other forms of $\Delta\mu(\sigma)$. In the fluid phase there is also a fixed-composition maximum volume fraction boundary: the random close packing volume fraction η_{RCP}. Schaertl and Sillesca [25] have studied η_{RCP} as a function of polydispersity. Their results are included in Fig. 6. The difference between the semigrand $\tilde{P}$ curve and the η_{RCP} curve is increasing with polydispersity. As in the solid case, this difference can be reduced by choosing other forms of the chemical potential distribution function. We demonstrate this via application of the hard-sphere mixture equation of state of Mansoori *et al.* [24], which is applicable to the fluid phase only. In Fig. 7, we plot the packing fraction versus polydispersity according to this equation of state, for the linear chemical potential distribution used in the simulations, and for distributions that are quadratic or cubic in the sphere diameter

$$\beta\Delta\mu(\sigma)=c_1\sigma+c_2\sigma^2+c_3\sigma^3, \tag{29}$$

where we have examined cases in which only one of c_1, c_2, and c_3 is nonzero. The figure simply shows how other chemical potential forms can give rise to larger densities than the ''infinite pressure'' results studied here. We note several points: (i) the case where $c_1=c_2=c_3=0$ results in a so-called infinitely polydisperse mixture [26], at which $s=0.7414$ and $\eta=0.104$; this situation arises as $\tilde{P}\to\infty$; (ii) the Mansoori equation agrees very well with the Monte Carlo data we have taken at and near the freezing transition, as well as at the infinitely polydisperse limit; however, one would not expect the equation to apply at conditions appropriate to random close packing, so we cannot describe this limit in the present analysis; (iii) the c_3 line is terminated at a point ($c_3/\beta P=0.507$) where the computed composition—which is an exponential of a cubic polynomial in σ—diverges because the coefficient of the cubic term becomes positive (the c_1 and c_2 lines are terminated on the figure at arbitrary points).

VIII. CONCLUSIONS

We have established a solid-fluid coexistence region for a system of polydisperse hard spheres with near-Gaussian diameter distributions, as a function of polydispersity. Our approach employs simulation in the isobaric semigrand ensemble with a Gaussian activity distribution. Gibbs-Duhem integration is used to trace the coexistence pressure as a function of the variance of the imposed activity distribution. The Gibbs-Duhem integration is initiated with a monodisperse hard-sphere fluid and fcc solid, and throughout the integration process the solid remains in an fcc structure. We do not explore the possibility of a polymorphic transition in the solid.

Both the fluid-solid coexistence densities and volume fractions are monotonically increasing functions of the polydispersity s, which is given in terms of the standard deviation in the particle diameter distribution function. The volume change at the freezing transition decreases as a function of s and eventually takes on negative values, which implies that the number density of the fluid phase is greater than that of the solid. However, the packing fraction of the fluid remains always less than that of the coexisting solid phase. Connected to this is the observation of significant fractionation between the two phases, which permits the fluid phase to comprise particles of a smaller average diameter.

Significantly, we observe a terminal polydispersity, i.e., a polydispersity above which there can be no fluid-solid coexistence. This terminus arises quite naturally as the Gibbs-

Duhem integration path leads the pressure to infinity. The existence of this terminus only at infinite pressure precludes the construction of a continuous path from the solid to the fluid. While it was anticipated in previous studies that such a continuous path could not be constructed, the issue was not addressed as fully as we are able to here.

At the terminus the polydispersity is 5.7% for the solid and 11.8% for the fluid while the volume fractions are 0.588 and 0.547 for the solid and fluid, respectively. Large fractionation observed at moderate values of $s(>0.05)$ implies that the constrained eutectic assumption implicit in previous studies is not valid over a very large range of polydispersity. The constrained eutectic approximation is perhaps the reason that McRay and Haymet [17] obtained the smaller value of 6% for the terminus. Our results for the terminal polydispersity are consistent with experiments performed on polydisperse colloidal suspensions.

We feel that the qualitative conclusion that a terminal polydispersity exists is generally correct and that it is of the order of 5% in the solid and 12% in the fluid. However, we have not examined the sensitivity of the terminal polydispersity to variation in the chemical potential distribution function (and thus the composition). It seems likely that the terminal polydispersity would not be very sensitive to details of composition, and as our distributions are near Gaussian we expect our conclusions to be generally valid.

ACKNOWLEDGMENTS

Acknowledgment is made to the Donors of the Petroleum Research Fund, administered by the American Chemical Society, for support of this research. Computing equipment was provided via support of the U.S. National Science Foundation, Grants CTS-9057161 and CTS-9212682; travel support has been provided by NATO. The authors wish to thank Germonda Mooij for a critical reading of the manuscript.

[1] J. P. Hansen and I. R. McDonald, *Theory of Simple Liquids* (Academic, London, 1986).
[2] W. G. Hoover and F. H. Ree, J. Chem. Phys. **49**, 3609 (1968).
[3] D. Frenkel and A. J. C. Ladd, J. Chem. Phys. **87**, 3188 (1984).
[4] X. Cottin and P. A. Monson, J. Chem. Phys. **99**, 8914 (1993).
[5] X. Cottin and P. A. Monson, J. Chem. Phys. **102**, 3354 (1995).
[6] M. D. Eldridge, P. A. Madden, and D. Frenkel, Nature **365**, 35 (1993).
[7] D. Frenkel, H. N. W. Lekkerkerker, and A. Stroobants, Nature **332**, 882 (1988).
[8] J. A. C. Veerman and D. Frenkel, Phys. Rev. A **41**, 3237 (1990).
[9] M. P. Allen, G. T. Evans, D. Frenkel, and B. M. Mulder, Adv. Chem. Phys. **86**, 1 (1993).
[10] W. B. Russel, D. A. Saville, and W. R. Schowalter, *Colloidal Dispersions* (Cambridge University Press, Cambridge, England, 1989).
[11] P. Pusey, in *Les Houches, Session LI, Liquids, Freezing and Glass Transitions, NATO Advanced Study Institute, Series B: Physics,* edited by J. P. Hansen, D. Levesque and J. Zinn-Justin (North-Holland, Amsterdam, 1991), Chap. 10.
[12] E. Dickinson, Discuss. Faraday Soc. **65**, 127 (1978).
[13] E. Dickinson, R. Parker and M. Lal, Chem. Phys. Lett. **79**, 578 (1981).
[14] E. Dickinson and R. Parker, J. Phys. Lett. **46**, L-229 (1985).
[15] P. Pusey, J. Phys. **48**, 709 (1987).
[16] J. L. Barrat and J. P. Hansen, J. Phys. **46**, 1547 (1986).
[17] R. McRae and A. D. J. Haymet, J. Chem. Phys. **88**, 1114 (1988).
[18] D. A. Kofke, J. Chem. Phys. **98**, 4149 (1993).
[19] J. G. Briano and E. D. Glandt, J. Chem. Phys. **80**, 3336 (1984).
[20] D. A. Kofke and E. D. Glandt, Mol. Phys. **64**, 1105 (1988).
[21] D. A. Kofke and E. D. Glandt, J. Chem. Phys. **87**, 4881 (1987).
[22] M. Metha and D. A. Kofke, Chem. Eng. Sci. **49**, 2633 (1994).
[23] B. Widom, J. Chem. Phys. **39**, 2808 (1963).
[24] G. A. Mansoori, N. F. Carnahan, K. E. Starling, and T. W. Leland, Jr., J. Chem. Phys. **54**, 1523 (1971).
[25] W. Schaertl and H. Sillescu, J. Stat. Phys. **77**, 1007 (1994).
[26] D. A. Kofke and E. D. Glandt, J. Chem. Phys. **90**, 439 (1988).